

# CoKe: Localized Contrastive Learning for Robust Keypoint Detection

Yutong Bai\*, Angtian Wang\*, Adam Kortylewski, Alan Yuille

Johns Hopkins University

{ytongbai, alan.l.yuille}@gmail.com; {angtianwang, akorty11}@jhu.edu

## Abstract

Today’s most popular approaches to keypoint detection learn a holistic representation of all keypoints. This enables them to implicitly leverage the relative spatial geometry between keypoints and thus to prevent false-positive detections due to local ambiguities. However, our experiments show that such holistic representations do not generalize well when the 3D pose of objects varies strongly, or when objects are partially occluded. In this paper, we propose *CoKe*, a framework for the supervised contrastive learning of *distinct local feature representations* for robust keypoint detection. In particular, we introduce a feature bank mechanism and update rules for keypoint and non-keypoint features which make possible to learn local keypoint detectors that are accurate and robust to local ambiguities. Our experiments show that CoKe achieves state-of-the-art results compared to approaches that jointly represent all keypoints holistically (Stacked Hourglass Networks, MSS-Net) as well as to approaches that are supervised with the detailed 3D object geometry (StarMap). Notably, CoKe performs exceptionally well when objects are partially occluded and outperforms related work on a range of diverse datasets (PASCAL3D+, ObjectNet, MPII).

## Introduction

Computer vision models are often deployed in safety-critical real-world applications, such as self-driving cars and security systems. In these application areas, we expect models to reliably generalize to previously unseen visual stimuli. However, in practice we observe that deep models do not generalize as well as humans in scenarios that are different from what has been observed during training, e.g., unseen partial occlusion, rare object pose, changes in the environment, etc.. This lack of generalization to *out-of-distribution* data may lead to fatal consequences in real-world applications, e.g. when driver-assistant systems fail to detect partially occluded pedestrians. Recent works (Zhu et al. 2019; Kortylewski et al. 2020b) have shown that deep vision systems are not as robust as humans to partial occlusion at image classification. Our experiments show that partial occlusion and a large variability in the 3D pose of objects, also poses a fundamental challenge for state-of-the-art keypoint detectors that needs to be addressed.

\*Joint first authors

Semantic keypoints, such as the joints of a human body, provide concise abstractions of visual objects in terms of their shape and pose. Accurate keypoint detections are of central importance for many visual understanding tasks, including viewpoint estimation (Pavlakos et al. 2017), human pose estimation (Cao et al. 2017), action recognition (Messing, Pal, and Kautz 2009), feature matching (Long, Zhang, and Darrell 2014), image classification (Zhang et al. 2014), and 3D reconstruction (Kanazawa et al. 2018). Early work on keypoint detection used independent detectors for each individual keypoint (Hamouz et al. 2005; Gourier, Hall, and Crowley 2004). However, such independent detectors cannot leverage structural information between keypoints to resolve local ambiguities. Therefore, they typically suffer from many false positive detections. This insight led to the development of keypoint detection approaches that represent the relative structure between keypoints either explicitly or implicitly. Approaches that explicitly model the spatial relationship between keypoints rely on prior knowledge about the object geometry, e.g. using mesh models (Bai et al. 2019). Such an explicit modeling is difficult because it either requires a careful hand-designed spatial structure between the keypoints (Felzenszwalb and Huttenlocher 2005; Chen and Yuille 2014) or additional supervision during training, in terms of the object viewpoint and a 3D mesh (Tulsiani and Malik 2015). Today’s most widely applied keypoint detection approaches (Yang et al. 2017; Chu et al. 2017; Ke et al. 2018) are based on the basic structure design of Stacked-Hourglass-Networks (Newell, Yang, and Deng 2016) (SHGs). A key idea in SHGs is that the model predicts the response maps of the keypoints jointly. At their core such models learn a joint representation of all keypoints, which allows them leverage the relative spatial geometry between the keypoints implicitly and hence makes possible to avoid the explicit modeling of the objects geometry. However, our experiments in Section show that for SHGs the occlusion of a few keypoints also strongly decreases the detection accuracy of the remaining visible keypoints due to the jointly entangled representation. Therefore, a critical research question is how to learn keypoint detectors that achieve a high performance and do not require any prior knowledge about the object geometry, while at the same time being very robust to partial occlusion.

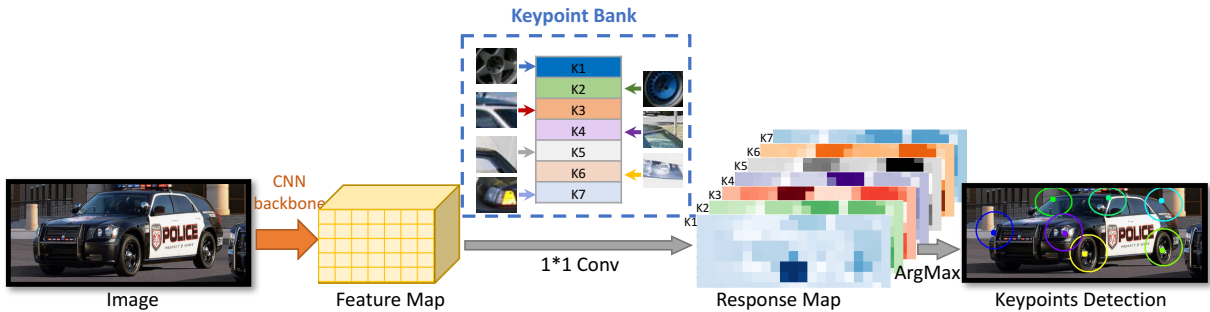


Figure 1: Keypoint detection with CoKe. We use a CNN backbone to extract feature representation at different positions of the input image. Each keypoint in the Keypoint Bank has an individual representation that is used as a convolution kernel to compute a response map for each keypoint. The location of maximum response is used as prediction result. The colored boxes show the ground truth and the dots illustrate the prediction result.

In this work, we learn keypoint detectors with separate local representations for every keypoint. This intuitively offers more robustness to partial occlusion compared to models that have a jointly entangled representation of all keypoints. However, a main challenge is to reduce the false-positive detections of the independent detectors due to local ambiguities in the image. To resolve this challenge, we introduce CoKe, a framework for learning independent keypoint detectors with localized representations via contrastive learning. Instead of following the regular supervised contrastive learning of holistic image representations, we aim to learn *local representations* that can perform fine-grained and accurate keypoint detection. In particular, we use the keypoint annotations to generate large amounts of negative examples and train a deep network backbone to distinguish between positive and negative examples locally. We introduce a contrastive loss for local features that enables a deep network to distinguish between representations of locally ambiguous keypoints. Additionally, we introduce a feature bank mechanism and update rules for keypoint and non-keypoint features which make possible to learn local keypoint detectors that are accurate and robust to local ambiguities.

In our experiments we show that CoKe achieves state-of-the-art results compared to approaches that jointly represent all keypoints holistically (Stacked Hourglass Networks, MSS-Net) as well as to approaches that are supervised with the detailed 3D object geometry (StarMap). This is remarkable as CoKe performs keypoint detection independently without any geometric constraints between the keypoints. Notably, due to the local representations in CoKe, the model performs exceptionally well when objects are partially occluded. It also enables CoKe to outperform related work on a range of diverse datasets (PASCAL3D+, ObjectNet, MPII), in particular in challenging scenarios such as when objects vary strongly in terms of their 3D pose.

## Related Work

**Keypoint Detection.** Keypoint detection, especially for human joints (Cao et al. 2017; Newell, Yang, and Deng 2016; Tompson et al. 2015; Toshev and Szegegy 2014) and rigid objects (Wu et al. 2016), is a widely studied problem in

computer vision. Early approaches relied on local descriptors (Gourier, Hall, and Crowley 2004) that are distinctive and invariant (Lowe 2004). While approaches using local descriptors have proven to be robust to occlusion and background clutter, they were outperformed by deep learning approaches that were trained end-to-end (Newell, Yang, and Deng 2016). Toshev et al. (Toshev and Szegegy 2014) first trained a deep neural network for 2D human pose regression and Li et al. (Li and Chan 2014) extended this approach to 3D. Starting from the work of Tompson et al. (Tompson et al. 2015), the heatmap representation became very popular for 2D keypoint estimation, achieving very good performances in both 2D human pose estimation (Newell, Yang, and Deng 2016) and category-specific object keypoint detection (Pavlakos et al. 2017). These works showed that predicting keypoints jointly with deep networks led to an improved performance, as the implicitly encoded structural information between keypoints provides important cues to resolve locally ambiguous keypoint detections. Tulsiani et al. (Tulsiani and Malik 2015), proposed to integrate the structural information between keypoints explicitly by integrating 2D and 3D models, which inspired a number of follow-up works, in particular for rigid objects (Zhou et al. 2018; Tulsiani and Malik 2015; Pavlakos et al. 2017).

**Supervised Contrastive Learning.** Contrastive learning originates from Metric Learning and involves the learning of a feature space by optimizing the similarities of sample pairs in a representation space. The general intuition underlying supervised contrastive learning is to transform the training data into a feature space where the distance of feature representations of samples from the same class is small, whereas it should be big for samples from different classes. Popular examples use pairs of samples for loss computation (Hadsell, Chopra, and LeCun 2006), triplets (Schroff, Kalenichenko, and Philbin 2015), or N-Pair tuples (Sohn 2016).

Recently, contrastive learning has attracted attention from the research community in self-supervised learning (Chen et al. 2020). The main difference in the self-supervised learning setting is that positive examples are generated using data augmentations of a query sample whereas negative examples are simply chosen as other images in the same mini-batch.

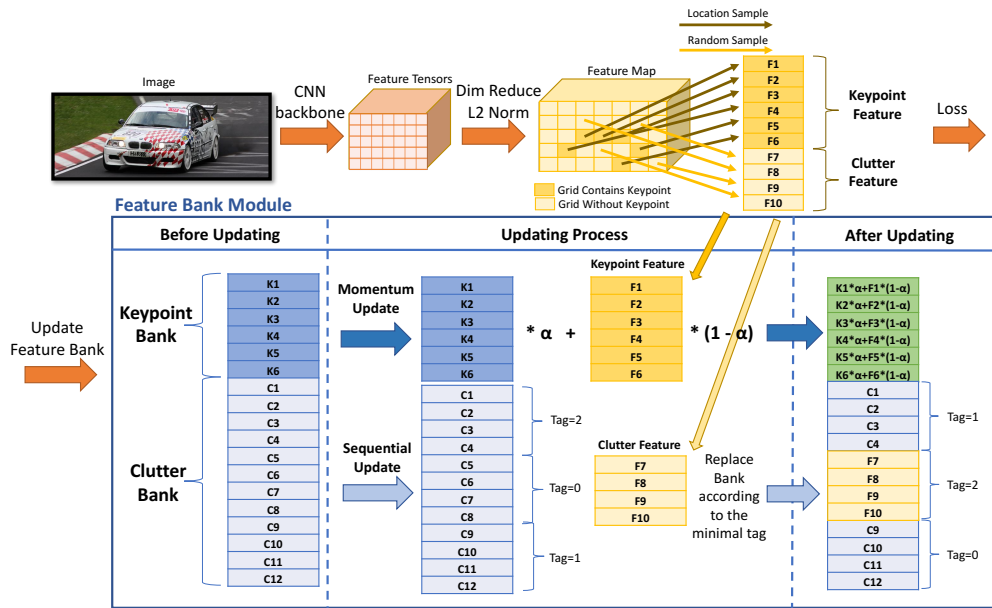


Figure 2: Illustration the CoKe training process. At first, we extract a feature map for the input image. After dimensionality reduction and  $L_2$  normalization, we retrieve the feature vectors for all keypoints as well as random clutter. We refer to these features as 'Keypoint Feature' and 'Clutter Feature'. We compute the loss between these features w.r.t. the Feature Bank Module and update the feature bank accordingly. The feature bank consists of two parts: a Keypoint Bank and a Clutter Bank. The Keypoint Bank is updated using momentum update. The Clutter Bank is updated by replacing the oldest features in the Clutter Bank with a set of randomly sampled clutter features from the input image based on the time tag. (Best viewed in color.)

While most of the supervised contrastive learning focuses on learning a holistic representation of the complete image, in this paper, we target a more fine-grained task - keypoint detection. Keypoints are localized image patterns and therefore require the learning of local feature embeddings. The main challenge is that local image patterns can be highly ambiguous (e.g. the front and back tire of a car) and therefore require a contrastive learning framework that can learn to disambiguate local representations, while at the same time being able to learn a distinct representation that can be localized accurately.

## CoKe: Contrastive Learning of Keypoint Detectors

In this section, we introduce CoKe, a framework for the contrastive learning of high performance keypoint detectors with individual representations. We give an overview over the inference process for a trained CoKe model in Section , and discuss the model training in detail in Section .

### Inference with the CoKe Model

In the following, we describe the model for keypoints of a single category. However, note that it can be easily extended to multiple categories. Figure 1 illustrates the keypoint detection process with the CoKe model after a successful training. The process can be summarized in three steps: feature extraction, keypoint matching and keypoint localization.

We compute the feature map of an image  $\mathbf{I}$  as:  $\mathbf{V} = f_{\theta}(\mathbf{I}) \in \mathbb{R}^{H \times W \times D}$ , where  $f_{\theta}$  is the feature extraction

with deep neural network backbone, followed by dimensionality reduction using a  $1 \times 1$  convolution and channel-wise  $L_2$ -normalization to project the feature vectors onto a unit hyper-sphere.  $\theta$  represents the trainable parameters of the backbone. Note that the CoKe approach does not depend on the particular architecture of the backbone (see experiments in Section ) and is hence able to benefit directly from advances in the architecture design.

In CoKe each keypoint has a separate representation  $K_n \in \mathbb{R}^D$ . We store all feature representations in a *Keypoint Bank*  $\mathbf{K} = \{K_n | n = 1, \dots, N\}$ . We assume a fixed number of  $N$  keypoints for each object class. For keypoint matching, we apply the keypoint representations from the Keypoint Bank as a  $1 \times 1$  convolution kernel. This computes the similarity between each keypoint representation and the features in the feature map  $\mathbf{V}$ . We compute the location of a keypoint  $n$  as the maximal response in the corresponding response map and project the detected location into the original image to get the final prediction result. As each point in the feature map projects onto a region in the input image, we simply choose the center of that region as final prediction in the input image.

Note the fundamental difference between CoKe and related work is that in CoKe each keypoint has its own representation, whereas e.g. in Stacked-Hourglass-Networks the representations of the keypoints are jointly entangled within the network parameters. The individual representation of keypoints in CoKe naturally enables robustness to occlusion, because the keypoints are detected independently dur-

ing inference and therefore occluded keypoints do not affect the detection of non-occluded keypoints. In contrast, when keypoint representations are entangled, partial occlusion of a few keypoints significantly decreases the detection accuracy of non-occluded keypoints, as illustrated in Figure 3 and shown in our experiments in Section .

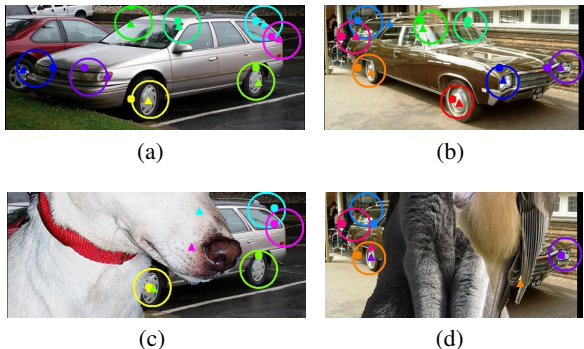


Figure 3: Negative effect of partial occlusion on keypoint localization. Colored Boxes: Ground truth keypoint location; Circles: CoKe predictions; Triangles: SHG predictions. For non-occluded objects (a & b) both models perform well. However, partial occlusion (c & d) distorts the SHGs because of the entangled keypoint representation, while CoKe can still localize the visible keypoints well.

### Training the CoKe Model

To train the CoKe model we introduce a contrastive framework that enables the learning of individual keypoint detectors with high discriminative performance. In the following, we introduce the components of the CoKe training process (Figure 2), including the keypoint and clutter feature extraction process, the Keypoint Bank, the Clutter Bank and the contrastive loss design.

**Extraction of Keypoint and Clutter Features.** Let  $\mathbf{V}_p \in \mathbb{R}^D$  denote the feature vector in the feature map  $\mathbf{V}$  at position  $p$ . A location  $X$  in the image  $\mathbf{I}$ , maps to a position  $p$  on feature map  $\mathbf{V}$ , such that  $p = \Phi(X)$ , where  $\Phi(\cdot)$  is the function that computes the mapping from  $X$  to  $p$ . For each keypoint, its position  $p_n$  on the feature map can be computed as  $p_n = \Phi(X_n)$ , where  $X_n$  is the keypoints' ground truth location in the 2D RGB image. We denote the feature vectors of all keypoints as  $\{\mathbf{F}_n = \mathbf{V}_{p_n} | n = 1, \dots, N\}$  and refer to this set as 'Keypoint Features'.

Our aim is to train the parameters of the feature extractor  $\theta$  such that the keypoint features  $F_n$  are distinct from each other, but also distinct from all other non-keypoint features in the image. To achieve this, we collect a set of background features that serve as negative examples during training. In particular, we randomly sample a set of 'Clutter Features'  $\{\mathbf{F}_m = \mathbf{V}_{p_m} | m = 1, \dots, M\}$  at positions  $p_m$  that are different from the keypoint positions, hence  $p_m \notin \{p_n | n = 1, \dots, N\}$ . A good clutter feature should be close to the keypoint annotation to reduce false-positive detections during inference at close by regions in the image.

Therefore, we use the ground truth keypoint annotation to sample clutter features within the vicinity of keypoint features (see Section for more details).

**Maintaining a Clutter Bank.** While the collection of ambiguous Clutter Features within a particular training image is effective, we found that it is important to maintain a record of Clutter Features from as many images as possible to ensure that the Keypoint Features will be distinct from all of them. Therefore, we store the Clutter Features in a *Clutter Bank*. In our experiments, a Clutter Bank consists of 1024 groups of features. Each group contains 20 Clutter Feature vectors. The dimensions of the Clutter Bank is chosen to fill up the memory the GPUs used for training. Typically, we observe that the bigger the Clutter Bank, the better the final performance (see experiments in Section ).

At first, we randomly initialize the Clutter Bank. For each training image, we put its Clutter Feature into the groups in Clutter Bank. After all the groups in the Clutter Bank are filled, we replace the 'oldest' group of Clutter Features based on a tag number that records the order in which the groups were filled. We refer to this process as *Sequential Update*.

### Contrastive Loss for Training the Feature Extractor.

The main challenge in the CoKe model is to reduce the false-positive detections of the independent detectors due to local ambiguities in the image. To achieve this we use a contrastive loss that is specifically designed to enhance the feature representations of the keypoints to be distinct from each other as well as from any other structures in the image. The loss is composed of three main terms:

$$\mathcal{L}(\{\mathbf{F}_n\}, \{\mathbf{F}_m\}, \mathbf{K}, \mathbf{C}) = \left[ \sum_n \mathcal{L}_{Key}(\mathbf{F}_n, \mathbf{K}_n) + \mathcal{L}_{Bank}(\mathbf{F}_n, \mathbf{K} \setminus \{\mathbf{K}_n\}, \mathbf{C}) \right] + \left[ \sum_m \mathcal{L}_{Clutter}(\mathbf{F}_m, \mathbf{K}) \right]. \quad (1)$$

The keypoint loss measures the cosine distance between the keypoint feature  $\mathbf{F}_n$  and the corresponding keypoint representation from the Keypoint Bank  $\mathbf{K}_n$ :

$$\mathcal{L}_{Key}(\mathbf{F}_n, \mathbf{K}_n) = -\mathbf{F}_n \mathbf{K}_n. \quad (2)$$

The bank loss measures the similarity between a particular Keypoint Feature  $\mathbf{F}_n$  to the Clutter Bank  $\mathbf{C}$  and all keypoint representations in the Keypoint Bank except the correct one  $\mathbf{K} \setminus \{\mathbf{K}_n\}$ :

$$\mathcal{L}_{Bank}(\mathbf{F}_n, \mathbf{K} \setminus \{\mathbf{K}_n\}, \mathbf{C}) = \left( \sum_{\mathbf{K} \setminus \{\mathbf{K}_n\}} \mathbf{F}_n \mathbf{K}_j + \sum_{\mathbf{C}} \mathbf{F}_n \mathbf{C}_i \right). \quad (3)$$

Finally, the clutter loss enforces the clutter features to have a large distance to all elements in the Keypoint Bank:

$$\mathcal{L}_{Clutter}(\mathbf{F}_m, \mathbf{K}) = \sum_n \mathbf{F}_m \mathbf{K}_n. \quad (4)$$

Note the difference to the bank loss is that it explicitly enforces the representation of the clutter to be distinct from the Keypoint Bank, whereas the bank loss only enforces the keypoint features to be different from the clutter features.

**Updating the Keypoint Bank.** We initialize the Keypoint Bank with random values sampled from a standard normal distribution. For every training image, we update the Keypoint Bank using momentum update. Note that, this mechanism is different from related work such as MoCo (He et al. 2019). In particular, CoKe uses momentum update to learn a category-specific feature representation, whereas MoCo uses momentum update to learn the weights of a backbone network.

$$\mathbf{K}_n \leftarrow \mathbf{K}_n * \alpha + \mathbf{F}_n * (1 - \alpha). \quad (5)$$

We set the momentum to  $\alpha = 0.9$  in our experiments. Note that we apply momentum updates, because they have proven to be more stable for contrastive learning compared to standard gradient descent updates (He et al. 2019).

## Experiments

In this section, we experimentally evaluate CoKe and compare its performance to related work that uses joint keypoint representations. We begin with describing the experimental setup in Section . We then evaluate the robustness of CoKe and other methods to partial occlusion in Section and perform ablation studies in Section .

### Experimental Setup

*Evaluation Protocol.* Following the standard experimental setup, we use PCK=0.1 (percentage of correct keypoints), as the evaluation metric. PCK considers a keypoint to be correct if its  $L_2$  pixel distance from the ground truth keypoint location is less than  $0.1 \cdot \max(h, w)$ , where  $h$  and  $w$  are the objects bounding box pixel size. We evaluate each object category by computing the average accuracy on the visible keypoints over all the test images.

*Training Setup.* For training we use a batch size of 64. In each image, we randomly choose 20 clutter points as a group and the clutter bank contains 1024 groups. We choose the clutter features to be within two pixels distance to the keypoint annotation in the feature map. We choose to use the non-parametric softmax (Wu et al. 2018) to calculate the similarity between features and banks. The temperature parameter(Hinton, Vinyals, and Dean 2015) that controls the concentration level of the distribution is set to  $\tau = 0.7$ . We compute the baseline following the basic settings of the Stacked Hourglass Network with 8 stacks.

*PASCAL3D+ Dataset.* We evaluate our approach on the PASCAL3D+ benchmark. The dataset contains 12 man-made object categories with totally 11045 images for training and 10812 images for evaluation. Different from some previous work (Zhou et al. 2018; Tulsiani and Malik 2015), we use all the images for evaluation, including the occluded and truncated ones. The number of keypoints ranges from 7 to 15 per category.

*OccludedPASCAL3D+ Dataset.* While it is important to evaluate algorithms on real images of partially occluded objects (see experiments in Section ), simulating occlusion enables us to quantify the effects of partial occlusion more accurately. Inspired by the success of dataset with artificially generated partial occlusion in image classification

PASCAL3D+					
Occlusion Lv	L0	L1	L2	L3	Avg
SHGs	68.0	46.5	43.2	39.9	49.4
MSS-Net	68.9	46.6	42.9	39.6	49.5
StarMap	78.6	-	-	-	-
CoKe-Res50	77.0	67.6	<b>59.9</b>	53.4	64.4
CoKe-SHG	78.3	66.3	58.4	52.3	63.8
CoKe-Res-UNet	<b>80.3</b>	<b>68.5</b>	59.1	<b>54.0</b>	<b>65.5</b>

Table 1: Keypoint detection results on PASCAL3D+ under different levels of partial occlusion (0%,20-40%,40-60%,60-80% of objects are occluded). CoKe models learned from several different backbones (ResNet50, Stacked-Hourglass, Res-UNet) are highly robust to partial occlusion. Furthermore, they outperform the models that leverage additional the structural information between the keypoints implicitly (SHGs, MSS-Net(Ke et al. 2018)) and explicitly (StarMap).

(Kortylewski et al. 2020b,a), part detection (Wang et al. 2017) and object detection (Wang et al. 2020) , we use an analogous dataset with artificial occlusion for keypoint detection. In particular, we use the *OccludedPASCAL3D+* dataset proposed in (Wang et al. 2020) for object detection. It contains all 12 classes of the original PASCAL 3D+ (Xiang, Mottaghi, and Savarese 2014) at various levels of occlusion. The occluders, include humans, animals and plants, which were cropped from the MS-COCO dataset (Lin et al. 2014) are different from the 12 PASCAL3D+ classes. The dataset has a total of 3 occlusion levels, with Lv.1: 20-40%, Lv.2: 40-60% and Lv.3: 60-80% of the object area being occluded.

*MPII Dataset.* MPII Human Pose (Andriluka et al. 2014) has 25k images with annotations for multiple people providing 40k annotated samples (28k training, 11k testing). MPII consists of images taken from a wide range of human activities with a challenging array of articulated poses. The keypoint visibility is annotated, which enables us to report numbers for the full dataset as well as partially occluded humans.

*ObjectNet3D Dataset.* ObjectNet3D (Xiang et al. 2016) consists of common objects in daily life and is notably more difficult compared to PASCAL3D+ as it contains more rare viewpoints, shapes and truncated objects. We use 14 randomly chosen classes from ObjectNet3D in our evaluation.

### Robustness to Partial Occlusion

**PASCAL3D+.** Table 1 shows the keypoint detection results on the PASCAL3D+ dataset for CoKe models learned from three different backbones: ResNet-50 (He et al. 2016), Stacked-Hourglass-Network (Newell, Yang, and Deng 2016) and Res-UNet (Zhang, Liu, and Wang 2018). The performance of the CoKe models with these very different backbones is constantly high. The highest performance is achieved with the most recently developed architecture Res-UNet. When compared to Stacked-Hourglass-Networks (SHGs) we can clearly observe a large gain in performance. Most notably, the performance difference is very promi-



Figure 4: Qualitative detection results under different levels of partial occlusion for artificially occluded objects from PASCAL3D+ (a-d) and humans from MPII (e). The dots visualize the detection result of CoKe. The colored circles in (a-d) indicate the ground-truth position within PCK=0.1. Note how CoKe is very robust even under strong occlusion.

Dataset	MPII		ObjectNet3D
	Full	Occluded	Full
CoKe-SHG	<b>90.3</b>	<b>85.1</b>	<b>49.8</b>
SHGs	90.1	84.3	48.6

Table 2: Keypoint detection results on MPII and ObjectNet3D with a Stacked-Hourglass-Network (SHGs) and a CoKe model learned from the SHGs backbone. CoKe outperforms SHGs on MPII, not only on the original images but challenging scenarios such as occluded humans as well. Also on the ObjectNet3D, a large-scale multi-class keypoint detection dataset.

ment for strong occlusion. We also report the performance of StarMap (Zhou et al. 2018) which uses explicit 3D models to jointly reason about the relative position of the keypoints. Note that StarMap reports only 2113 images which are non-truncated and non-occluded, but we report results for all 11476 images without manually picking up. Overall, our results clearly highlight that CoKe is competitive with models that leverage geometric constraints between keypoints either explicitly or implicitly, while being highly robust to partial occlusion

**MPII and ObjectNet3D.** We compare Stacked-Hourglass-Networks and a CoKe model learned from the SHGs backbone on MPII and ObjectNet3D in Table 2. CoKe-SHG outperforms SHGs for both human keypoint detection on the MPII dataset and object keypoint detection on ObjectNet3D dataset.

In summary, we observe that CoKe is a general purpose

framework that constantly achieves a high performance for a wide range of backbone architectures and for a range of datasets with very different characteristics.

**Qualitative Results.** We visualize qualitative results in Figure 4. Overall, the illustrations demonstrate the robustness of CoKe to partial occlusions. Any keypoints that are not in the vicinity of occluders are correctly detected and not affected by the occlusion. Furthermore, keypoints that are partially occluded (e.g. the wheel) can still be located robustly, although the detections tend to move away from the occluder. Importantly, we do not observe false positive detections at locally ambiguous keypoints. This demonstrates that CoKe leverages the large receptive field to disambiguate keypoints, while still being able to localize individual keypoints accurately.

**Time and Memory Consumption.** During inference, CoKe-Res50 (params: 23M, acc: 77%) takes 0.01s per image, while (SHGs) (params: 25M, acc: 68%) needs 0.06s per image. For the memory consumption, CoKe-Res50 needs 715MB, SHGs 786MB when batch size equals to 1. CoKe has an advantage of the inference time while maintaining the competence of the memory consumption.

**Feature Map Visualization.** Here we also provide some visualization of the feature map from CoKe-Res50. All of them are from Car category which has more images and more complex situations in PASCAL3D+. From the Figure 5 we can observe that CoKe is robust to challenging scenarios. It is worth noting that how all keypoints are detected accurately despite the difficulty from false positives, occlusions, rare viewpoints, different domain, irregular appearance and irregular state and rare viewpoints.

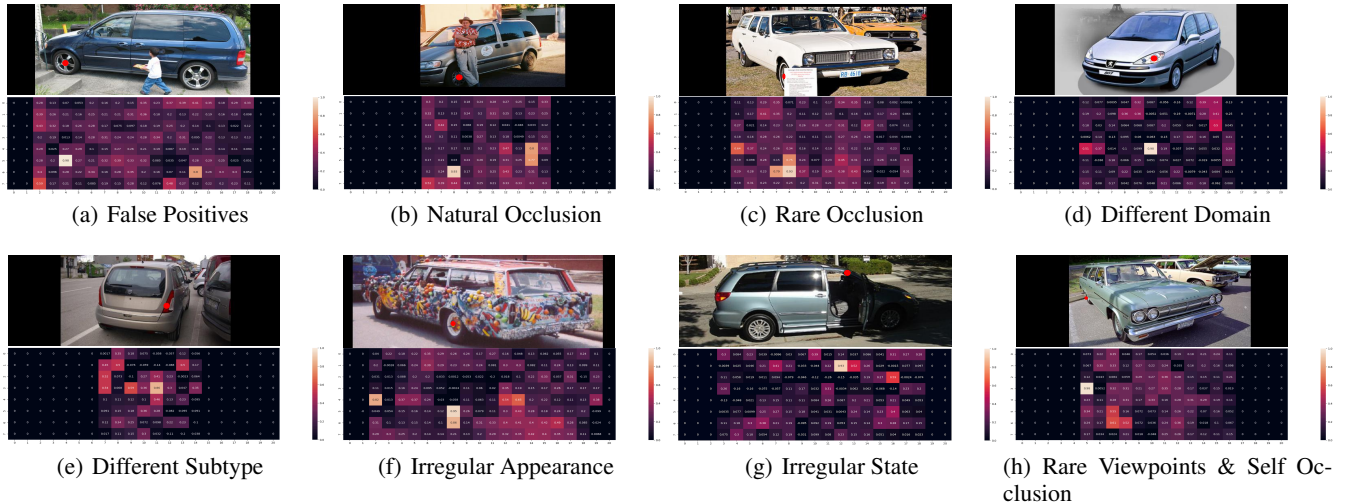


Figure 5: Eight examples of CoKe-Res50’s representation visualization. For each sub-figure, top is the original image with keypoint annotation, labeled with red dot. Bottom is the response map, predicted by CoKe-Res50. It is worth noting that how all keypoints are detected accurately despite the difficulty from false positives, occlusions, rare viewpoints, different domain, irregular appearance and irregular state and rare viewpoints. (Best viewed in color.)

### Ablation Study

In Table 3, we study the influence of the clutter features and the clutter loss on the contrastive learning result. In particular, it shows the keypoint detection results for CoKe-Res-UNet on the car category of the PASCAL3D+ dataset. We observe that the performance decreases significantly when no clutter features are used during training. An extension of this basic setup is to use image-specific clutter features but without maintaining the features in a Clutter Bank. In particular, we select the clutter features from the same image from which the keypoint features are sampled using the same hard negative sampling mechanism as in our standard setup. From the results we observe that using the image-specific clutter features increases the performance significantly. However, the best performance is achieved using our proposed Clutter Bank mechanism. In particular, the results show a general trend that the more features we store in the bank, the higher the performance becomes. Notably, lower occlusion scenarios benefit from a larger clutter bank while for stronger occlusion a smaller clutter bank is more beneficial. Finally, our ablation shows that explicitly regularizing the clutter to be distinct from the Keypoint Bank using the clutter loss (Equation 4) is highly beneficial.

### Conclusion

In this work, we considered the problem of robust keypoint detection. We found that a key problem of today’s most popular approaches is that they model all keypoints in a holistic, jointly entangled representation. In an effort to resolve this limitation, we made the following contributions:

**CoKe - A localized contrastive learning framework for keypoint detectors.** Instead of modeling keypoints jointly in a holistic representation, we learned an independent local feature representation for every keypoint. In particular, we

Occlusion Level	L0	L1	L2	L3
No clutter	79.3	75.4	71.8	65.8
Image-specific clutter	92.8	82.7	76.5	69.2
Clutter Bank (64 groups)	93.0	83.6	<b>80.1</b>	<b>73.3</b>
Clutter Bank (256 groups)	94.3	84.3	77.7	71.0
Clutter Bank (1024 groups)	<b>95.5</b>	<b>85.9</b>	79.0	70.6
Clutter Bank (1024 groups) w/o clutter loss	94.2	83.1	76.8	68.0

Table 3: Ablation study on PASCAL3D+ with different settings for contrastive learning using: no clutter features, image-specific clutter features (using 20 features from the same image as negative examples), our proposed Clutter Bank with different number of groups, where each group contains 20 features and when deactivating the clutter loss. Note the benefit of using clutter features in general, and in particular using a large clutter bank, as well as the importance of the clutter loss.

introduced a contrastive loss that enabled a deep network to distinguish between representations of locally ambiguous keypoints. In addition, we introduced a bank mechanism for keypoint and non-keypoint features to enhance models’ robustness to false-positive detections in background regions.

**General-purpose keypoint detection with robustness to partial occlusion.** Our experiments show that CoKe is a general-purpose framework that achieves a constantly high performance for a wide variety of backbone architectures and for a range of datasets with very different characteristics. We also demonstrate that CoKe detectors can localize keypoints of partially occluded objects more accurately compared to popular approaches that use jointly entangled representations of keypoints.

## Broader Impact

In general, enabling computer vision systems to be robust to partial occlusion is highly beneficial for a broad range of real-world applications. Keypoint detection, in particular, serves as the basis for a number of computer vision tasks such as human pose estimation, action recognition or 3D reconstruction. Therefore we can expect that these tasks will also become more robust to partial occlusion. This will significantly advance the ability of autonomous agents to robustly perceive real-world environments. We see a multitude of potential application areas with positive societal impact such as e.g. self-driving cars or humanoid robotics. However, one should be aware that advances in computer vision in general, but also with respect to robustness to partial occlusion in particular, are also highly useful in controversial application areas such as military usage or the fully automated analysis of partially occluded humans in surveillance scenarios.

## References

- Andriluka, M.; Pishchulin, L.; Gehler, P.; and Schiele, B. 2014. 2D Human Pose Estimation: New Benchmark and State of the Art Analysis. In *IEEE Conference on Computer Vision and Pattern Recognition (CVPR)*.
- Bai, Y.; Liu, Q.; Xie, L.; Qiu, W.; Zheng, Y.; and Yuille, A. L. 2019. Semantic Part Detection via Matching: Learning to Generalize to Novel Viewpoints from Limited Training Data. In *Proceedings of the IEEE International Conference on Computer Vision*, 7535–7545.
- Cao, Z.; Simon, T.; Wei, S.-E.; and Sheikh, Y. 2017. Realtime multi-person 2d pose estimation using part affinity fields. In *Proceedings of the IEEE Conference on Computer Vision and Pattern Recognition*, 7291–7299.
- Chen, T.; Kornblith, S.; Norouzi, M.; and Hinton, G. 2020. A simple framework for contrastive learning of visual representations. *arXiv preprint arXiv:2002.05709*.
- Chen, X.; and Yuille, A. L. 2014. Articulated pose estimation by a graphical model with image dependent pairwise relations. In *Advances in neural information processing systems*, 1736–1744.
- Chu, X.; Yang, W.; Ouyang, W.; Ma, C.; Yuille, A. L.; and Wang, X. 2017. Multi-context attention for human pose estimation. In *Proceedings of the IEEE Conference on Computer Vision and Pattern Recognition*, 1831–1840.
- Felzenszwalb, P. F.; and Huttenlocher, D. P. 2005. Pictorial structures for object recognition. *International journal of computer vision* 61(1): 55–79.
- Gourier, N.; Hall, D.; and Crowley, J. L. 2004. Facial features detection robust to pose, illumination and identity. In *2004 IEEE International Conference on Systems, Man and Cybernetics (IEEE Cat. No. 04CH37583)*, volume 1, 617–622. IEEE.
- Hadsell, R.; Chopra, S.; and LeCun, Y. 2006. Dimensionality reduction by learning an invariant mapping. In *2006 IEEE Computer Society Conference on Computer Vision and Pattern Recognition (CVPR'06)*, volume 2, 1735–1742. IEEE.
- Hamouz, M.; Kittler, J.; Kamarainen, J.-K.; Paalanen, P.; Kalviainen, H.; and Matas, J. 2005. Feature-based affine-invariant localization of faces. *IEEE transactions on pattern analysis and machine intelligence* 27(9): 1490–1495.
- He, K.; Fan, H.; Wu, Y.; Xie, S.; and Girshick, R. 2019. Momentum contrast for unsupervised visual representation learning. *arXiv preprint arXiv:1911.05722*.
- He, K.; Zhang, X.; Ren, S.; and Sun, J. 2016. Deep residual learning for image recognition. In *Proceedings of the IEEE conference on computer vision and pattern recognition*, 770–778.
- Hinton, G.; Vinyals, O.; and Dean, J. 2015. Distilling the knowledge in a neural network. *arXiv preprint arXiv:1503.02531*.
- Kanazawa, A.; Tulsiani, S.; Efros, A. A.; and Malik, J. 2018. Learning category-specific mesh reconstruction from image collections. In *Proceedings of the European Conference on Computer Vision (ECCV)*, 371–386.
- Ke, L.; Chang, M.-C.; Qi, H.; and Lyu, S. 2018. Multi-scale structure-aware network for human pose estimation. In *Proceedings of the European Conference on Computer Vision (ECCV)*, 713–728.
- Kortylewski, A.; He, J.; Liu, Q.; and Yuille, A. 2020a. Compositional Convolutional Neural Networks: A Deep Architecture with Innate Robustness to Partial Occlusion. In *Proceedings of the IEEE Conference on Computer Vision and Pattern Recognition*.
- Kortylewski, A.; Liu, Q.; Wang, H.; Zhang, Z.; and Yuille, A. 2020b. Combining Compositional Models and Deep Networks For Robust Object Classification under Occlusion. In *The IEEE Winter Conference on Applications of Computer Vision*, 1333–1341.
- Li, S.; and Chan, A. B. 2014. 3d human pose estimation from monocular images with deep convolutional neural network. In *Asian Conference on Computer Vision*, 332–347. Springer.
- Lin, T.-Y.; Maire, M.; Belongie, S.; Hays, J.; Perona, P.; Ramanan, D.; Dollár, P.; and Zitnick, C. L. 2014. Microsoft coco: Common objects in context. In *European conference on computer vision*, 740–755. Springer.
- Long, J. L.; Zhang, N.; and Darrell, T. 2014. Do convnets learn correspondence? In *Advances in neural information processing systems*, 1601–1609.
- Lowe, D. G. 2004. Distinctive image features from scale-invariant keypoints. *International journal of computer vision* 60(2): 91–110.
- Messing, R.; Pal, C.; and Kautz, H. 2009. Activity recognition using the velocity histories of tracked keypoints. In *2009 IEEE 12th international conference on computer vision*, 104–111. IEEE.
- Newell, A.; Yang, K.; and Deng, J. 2016. Stacked hourglass networks for human pose estimation. In *European conference on computer vision*, 483–499. Springer.

- Pavlakos, G.; Zhou, X.; Chan, A.; Derpanis, K. G.; and Daniilidis, K. 2017. 6-dof object pose from semantic keypoints. In *2017 IEEE international conference on robotics and automation (ICRA)*, 2011–2018. IEEE.
- Schroff, F.; Kalenichenko, D.; and Philbin, J. 2015. Facenet: A unified embedding for face recognition and clustering. In *Proceedings of the IEEE conference on computer vision and pattern recognition*, 815–823.
- Sohn, K. 2016. Improved deep metric learning with multi-class n-pair loss objective. In *Advances in neural information processing systems*, 1857–1865.
- Tompson, J.; Goroshin, R.; Jain, A.; LeCun, Y.; and Bregler, C. 2015. Efficient object localization using convolutional networks. In *Proceedings of the IEEE Conference on Computer Vision and Pattern Recognition*, 648–656.
- Toshev, A.; and Szegedy, C. 2014. Deeppose: Human pose estimation via deep neural networks. In *Proceedings of the IEEE conference on computer vision and pattern recognition*, 1653–1660.
- Tulsiani, S.; and Malik, J. 2015. Viewpoints and keypoints. In *Proceedings of the IEEE Conference on Computer Vision and Pattern Recognition*, 1510–1519.
- Wang, A.; Sun, Y.; Kortylewski, A.; and Yuille, A. 2020. Robust Object Detection under Occlusion with Context-Aware CompositionalNets. In *Proceedings of the IEEE Conference on Computer Vision and Pattern Recognition*.
- Wang, J.; Xie, C.; Zhang, Z.; Zhu, J.; Xie, L.; and Yuille, A. 2017. Detecting semantic parts on partially occluded objects. *arXiv preprint arXiv:1707.07819* .
- Wu, J.; Xue, T.; Lim, J. J.; Tian, Y.; Tenenbaum, J. B.; Torralba, A.; and Freeman, W. T. 2016. Single image 3d interpreter network. In *European Conference on Computer Vision*, 365–382. Springer.
- Wu, Z.; Xiong, Y.; Yu, S. X.; and Lin, D. 2018. Unsupervised feature learning via non-parametric instance discrimination. In *Proceedings of the IEEE Conference on Computer Vision and Pattern Recognition*, 3733–3742.
- Xiang, Y.; Kim, W.; Chen, W.; Ji, J.; Choy, C.; Su, H.; Mottaghi, R.; Guibas, L.; and Savarese, S. 2016. Objectnet3d: A large scale database for 3d object recognition. In *European Conference on Computer Vision*, 160–176. Springer.
- Xiang, Y.; Mottaghi, R.; and Savarese, S. 2014. Beyond pascal: A benchmark for 3d object detection in the wild. In *IEEE winter conference on applications of computer vision*, 75–82. IEEE.
- Yang, W.; Li, S.; Ouyang, W.; Li, H.; and Wang, X. 2017. Learning feature pyramids for human pose estimation. In *proceedings of the IEEE international conference on computer vision*, 1281–1290.
- Zhang, N.; Donahue, J.; Girshick, R.; and Darrell, T. 2014. Part-based R-CNNs for fine-grained category detection. In *European conference on computer vision*, 834–849. Springer.
- Zhang, Z.; Liu, Q.; and Wang, Y. 2018. Road extraction by deep residual u-net. *IEEE Geoscience and Remote Sensing Letters* 15(5): 749–753.
- Zhou, X.; Karpur, A.; Luo, L.; and Huang, Q. 2018. Starmap for category-agnostic keypoint and viewpoint estimation. In *Proceedings of the European Conference on Computer Vision (ECCV)*, 318–334.
- Zhu, H.; Tang, P.; Park, J.; Park, S.; and Yuille, A. 2019. Robustness of Object Recognition under Extreme Occlusion in Humans and Computational Models. *CogSci Conference* .